Inorganic Chemistry
Article

Inorg. Chem. **2010**, *49*, 1699–1704 **1699**
DOI: 10.1021/ic902104r

In-Situ Powder X-ray Diffraction Investigation of Reaction Pathways for the $BaCO_3-CeO_2-In_2O_3$ and $CeO_2-In_2O_3$ Systems

Surinderjit Singh Bhella,[†] Shahid P. Shafi,[‡] Francesca Trobec,[†] Mario Bieringer,*[,‡] and Venkataraman Thangadurai*[,†]

[†]*Department of Chemistry, University of Calgary, Calgary, AB, T2N 1N4, Canada, and* [‡]*Department of Chemistry, University of Manitoba, Winnipeg, MB, R3T 2N2, Canada*

Received October 23, 2009

We report the first in-situ powder X-ray diffraction (PXRD) study of the $BaCO_3-CeO_2-In_2O_3$ and $CeO_2-In_2O_3$ systems in air over a wide range of temperature between 25 and 1200 °C. Herein, we are investigating the formation pathway and chemical stability of perovskite-type $BaCe_{1-x}In_xO_{3-\delta}$ ($x = 0.1$, 0.2, and 0.3) and corresponding fluorite-type $Ce_{1-x}In_xO_{2-\delta}$ phases. The potential direct solid state reaction between CeO_2 and In_2O_3 for the formation of indium-doped fluorite-type phase is not observed even up to 1200 °C in air. The formation of the $BaCe_{1-x}In_xO_{3-\delta}$ perovskite structures was investigated and rationalized using in-situ PXRD. Furthermore the decomposition of the indium-doped perovskites in CO_2 is followed using high temperature diffraction and provides insights into the reaction pathway as well as the thermal stability of the $Ce_{1-x}In_xO_{3-\delta}$ system. In CO_2 flow, $BaCe_{1-x}In_xO_{3-\delta}$ decomposes above $T = 600$ °C into $BaCO_3$ and $Ce_{1-x}In_xO_{2-\delta}$. Furthermore, for the first time, the in-situ PXRD confirmed that $Ce_{1-x}In_xO_{2-\delta}$ decomposes above 800 °C and supported the previously claimed metastability. The maximum In-doping level for CeO_2 has been determined using PXRD. The lattice constant of the fluorite-type structure $Ce_{1-x}In_xO_{2-\delta}$ follows the Shannon ionic radii trend, and crystalline domain sizes were found to be dependent on indium concentration.

1. Introduction

CeO_2 crystallizes in the fluorite-type structure and provides ample opportunities for doping with divalent and trivalent cations resulting in the solid solutions of $Ce_{1-x}M_xO_{2-\delta}$ (M = Ca, Sr, Ba, Ln = rare earth). The solid solutions are particularly interesting as potential solid oxide ion electrolytes with emerging applications in solid oxide fuel cells (SOFCs) and diverse gas sensors for gases such as oxygen, hydrocarbons, and hydrogen.[1−10] During the past two decades research has focused on correlating synthetic methods, chemical compositions, microstructures, and electrical transport properties in an effort to optimize the ionic and electronic conductivity of doped CeO_2.[11−19] Among them, 10 to 20 mol % Ln-doped $Ce_{1-x}Ln_xO_{2-\delta}$ have drawn much attention because of their high oxide ion conductivity compared to that of Y_2O_3-doped ZrO_2 (YSZ) and SrO+MgO-doped $LaGaO_3$ (LSGM).[6−10] Our continuing interests in the development of fast oxide ion conducting solid electrolytes has resulted in the recent preparation of rare earth and alkaline-doped $Ce_{1-x}M_xO_{2-\delta}$ (M = Y, Ca+Sm, Sm) through high temperature reactions of the corresponding $BaCe_{1-x}M_xO_{3-\delta}$ perosvkite phases in CO_2.[20−23]

*To whom correspondence should be addressed. E-mail: mario_bieringer@umanitoba.ca (M.B.), vthangad@ucalgary.ca (V.T.). Phone: 001 204 474 6258 (M.B.), 001 403 210 8649 (V.T.). Fax 001 204 474 7608.(M.B.), 001 403 289 9488 (V.T.).

(1) Subbarao, E. C.; Maiti, H. S. *Solid State Ionics* **1984**, *11*, 317–338.
(2) Inaba, H.; Tagawa, H. *Solid State Ionics* **1996**, *83*, 1–16.
(3) Boivin, J. C.; Mairesse, G. *Chem. Mater.* **1998**, *10*, 2870–2888.
(4) Mogensen, M.; Sammes, N. M.; Tompsett, G. A. *Solid State Ionics* **2000**, *129*, 63–94.
(5) Goodenough, J. B. *Annu. Rev. Mater. Res.* **2003**, *33*, 91–128.
(6) Weber, A.; Tiffee, E. I. *J. Power Sources* **2004**, *127*, 272–283.
(7) Kharton, V. V.; Marques, F. M. B.; Atkinson, A. *Solid State Ionics* **2004**, *174*, 135–149.
(8) Wincewicz, K. C.; Cooper, J. S. *J. Power Sources* **2005**, *140*, 280–296.
(9) Fergus, J. W. *J. Power Sources* **2006**, *162*, 30–40.
(10) Lashtabeg, A.; Skinner, S. J. *J. Mater. Chem.* **2006**, *16*, 3161–3170.
(11) Steele, B. C. H. *Solid State Ionics* **2000**, *129*, 95–110.
(12) Huang, W.; Shuk, P.; Greenblatt, M. *Chem. Mater.* **1997**, *9*, 2240–2245.
(13) Huang, W.; Greenblatt, M. *Solid State Ionics* **1997**, *100*, 23–27.
(14) Huang, K.; Feng, M.; Goodenough, J. B. *J. Am. Ceram. Soc.* **1998**, *81*, 357–362.
(15) Eguchi, K. *J. Alloys Compd.* **1997**, *250*, 486–491.
(16) Eguchi, K.; Setoguchi, T.; Inoue, T.; Arai, H. *Solid State Ionics* **1992**, *52*, 165–172.
(17) Yahiro, H.; Eguchi, Y.; Eguchi, K.; Arai, H. *J. Appl. Electrochem.* **1988**, *18*, 527–531.
(18) Matsui, T.; Inaba, M.; Mineshige, A.; Ogumi, Z. *Solid State Ionics* **2005**, *176*, 647–654.
(19) Kilner, J. A.; Waters, C. D. *Solid State Ionics* **1982**, *6*, 252–259.
(20) Sneha, B. R.; Thangadurai, V. *J. Solid State Chem.* **2007**, *180*, 2661–2666.
(21) Trobec, F.; Thangadurai, V. *Inorg. Chem.* **2008**, *47*, 8972–8984.
(22) Pearce, M. C.; Thangadurai, V. *Asia-Pac. J. Chem. Eng.* **2009**, *4*, 33–44.
(23) Gerlach, R. G.; Bhella, S. S.; Thangadurai, V. *Inorg. Chem.* **2009**, *48*, 257–266.

Published on Web 01/22/2010

Although a large number of studies were performed to substitute divalent and trivalent metal ions in CeO_2,[11−19] our attempt to substitute trivalent In for Ce by a conventional ceramic method was not successful in the temperature range of 800 °C−1500 °C.[21,22] It is noteworthy that based on the Shannon ionic radii, one would predict that doping In ($In^{3+}_{(VIII)}$ = 0.92 Å) for Ce ($Ce^{4+}_{(VIII)}$ = 0.97 Å) in the fluorite structure should be possible because the difference in ionic radii between In and Ce is 0.05 Å, almost half compared to that between Sm ($Sm^{3+}_{(VIII)}$ = 1.079 Å) and Ce.[24] The CeO_2 fluorite structure consists of Ce^{4+} ions forming a cubic close packed structure with O^{2-} ions in the tetrahedral interstitial sites, and each Ce^{4+} cation is surrounded by eight oxide ions. Pure In_2O_3 crystallizes in the bixbyite structure in space group $Ia\bar{3}$. Removal of two anions along the cubic body diagonal of the fluorite structure will result in the bixbyite structure; hence CeO_2 and In_2O_3 are structurally related. Surprisingly the direct synthesis of In-doped CeO_2 was not successful. Instead a two step synthesis involving first the formation of $BaCe_{1-x}In_xO_{3-\delta}$ and a subsequent treatment under CO_2 at 800 °C yielded $BaCO_3$ and the target compounds $Ce_{1-x}In_xO_{2-\delta}$. The $BaCO_3$ is being removed by acid wash.[21]

To understand the thermodynamic stability of the present In-doped cerates prepared via the CO_2 capture technique, the acid washed products were sintered in air at various temperatures. All products heated above 800 °C showed the presence of In_2O_3 indicating the decomposition of the $Ce_{1-x}In_xO_{2-\delta}$ into its corresponding metal oxides In_2O_3 and CeO_2. The In_2O_3 concentration increased with increasing sintering temperature. Consequently, the $Ce_{0.9}In_{0.1}O_{1.95}$ and $Ce_{0.8}In_{0.2}O_{1.9}$ appear to be metastable and cannot be prepared directly from CeO_2 and In_2O_3. The low temperature (800 °C) CO_2 mediated reaction performed on the In-doped Ba cerates provides an elegant alternative route for the preparation of $Ce_{1-x}In_xO_{2-\delta}$.[21]

All our previous investigations for the formation of $Ce_{1-x}In_xO_{2-\delta}$ have been carried out ex-situ; thus, no insights regarding the reaction pathway during the synthesis are available.[21] In-situ X-ray diffraction is an excellent probe for structural variations during phase transitions and solid state chemical reactions. The method permits identification of metastable intermediates that may not be accessible through quenching and allows the preparation of yet-unknown phases that have been missed because of poorly chosen ex-situ synthesis conditions.[25−27] Here, we report for the first time, the in-situ formation of the solid solution $BaCe_{1-x}In_xO_{3-\delta}$ (x = 0.1, 0.2, 0.3) and the subsequent CO_2 capture reaction during $Ce_{1-x}In_xO_{2-\delta}$ formation using real time in-situ powder X-ray diffraction (PXRD). Furthermore, the direct reaction between CeO_2 and In_2O_3 was followed by in-situ XRD and is being contrasted with the CO_2 capture reaction. We have explored the maximum indium-doping levels and provide a detailed description of the indium concentration dependent evolution of the $Ce_{1-x}In_xO_{2-\delta}$ fluorite-type phase.

2. Experimental Section

2.1. Synthesis of Bulk Samples. The $BaCe_{1-x}In_xO_{3-\delta}$ perovskite phases with $x \leq 0.4$ were synthesized by conventional solid-state reactions of stoichiometric amounts of $BaCO_3$ (Alfa Aeasar, 99.95%), CeO_2 (Alfa Aesar, 99.99%), and In_2O_3 (Alfa Aesar, 99.995%) for 6 h at 1200 °C according to eq 1.

$$BaCO_3 + (1-x)CeO_2 + (x/2)In_2O_3 \rightarrow BaCe_{1-x}In_xO_{3-\delta} + CO_2 \quad (1)$$

The starting materials were ground together in an agate mortar in acetone slurry, and the reactions were carried out in alumina crucibles. Fluorite-type phases of composition $Ce_{1-x}In_xO_{2-\delta}$ ($0.0 \leq x \leq 0.20$) were synthesized by heating the corresponding barium perovskite phases at 800 °C for 6 h in CO_2 flow according to eq 2.

$$BaCe_{1-x}In_xO_{3-\delta} + CO_2 \rightarrow Ce_{1-x}In_xO_{2-\delta} + BaCO_3 \quad (2)$$

The CO_2 capture reactions for $x > 0.2$ were carried out using the same procedure as described above for $x \leq 0.2$, but required lower reaction temperatures of T = 700 °C to avoid the formation of In_2O_3 as a decomposition product of the fluorite-type phase. In-situ PXRD experiments provided guidelines for the optimization of the CO_2 capture temperatures. The products obtained from CO_2 capture reactions were washed with 5% aqueous HCl to remove $BaCO_3$ and dried in a dynamic vacuum at room temperature.

2.2. PXRD. Room temperature powder X-ray diffractograms were collected on polycrystalline products mounted on Si (111) zero background sample holders using a PANalytical X'Pert Pro diffractometer in Bragg−Brentano configuration. Using Cu $K\alpha_{1,2}$ radiation, a diffracted beam Ni-filter and an X'Celerator detector diffractograms were collected from 2θ = 10° to 2θ = 90° in 0.0167° steps. Structure analysis was carried out with the Rietveld method using FullProf.2k.[28]

2.3. In-Situ PXRD. In-situ PXRD experiments were carried out on a PANalytical X'Pert Pro diffractometer equipped with an X'Celerator detector, a diffracted beam Ni filter and an Anton Paar HTK2000 high temperature attachment. For the formation of the $BaCe_{1-x}In_xO_{3-\delta}$ phases, stoichiometric samples of $BaCO_3$, CeO_2, and In_2O_3 were mounted as thin layers directly onto the resistive platinum strip heater and heated in 25 °C increments from 25 to 1200 °C in air. The temperatures of the furnace are accurate within ±5 °C. The perovskite decomposition for the formation of $Ce_{1-x}In_xO_{2-\delta}$ was followed using the same experimental set up and conditions in 1 atm of flowing CO_2. Using Cu $K\alpha_{1,2}$ radiation (λ = 1.540598, 1.544426 Å) 20 min diffraction data sets were collected at 0.0167° steps from 2θ = 17° to 2θ = 65°. Only impurity free perovskite phases (obtained via bulk synthesis) were used as starting materials for the in-situ CO_2 capture reactions.

3. Results and Discussion

3.1. Direct Reaction Between CeO_2 and In_2O_3. Previous attempts to dope CeO_2 with In^{3+} directly using ex-situ conventional solid state methods were not successful.[21] The direct reaction between 0.9 mol CeO_2 and 0.05 mol In_2O_3 was investigated using high temperature in-situ PXRD from 25 to 1100 °C in 25 °C increments in air. Figure 1 shows the PXRD contour plot indicating concerted peak shifts of CeO_2 and In_2O_3 toward smaller 2θ angles with increasing temperature consistent with thermal expansion of both phases. Note that the CeO_2 peaks

(24) Shannon, R. D. *Acta Crystallogr.* **1976**, *A32*, 751–767.
(25) Lundgren, R. J.; Cranswick, L. M. D.; Bieringer, M. *J. Solid State Chem.* **2006**, *179*, 3599–3606.
(26) Lundgren, R. J.; Cranswick, L. M. D.; Bieringer, M. *Chem. Mater.* **2007**, *19*, 3945–3955.
(27) Shafi, S. P.; Lundgren, R. J.; Cranswick, L. M. D.; Bieringer, M. *J. Solid State Chem.* **2007**, *180*, 3333–3340.
(28) J. Rodriguez- Carvajal, *FullProf.2k*, Vers. 4.40, 2008.

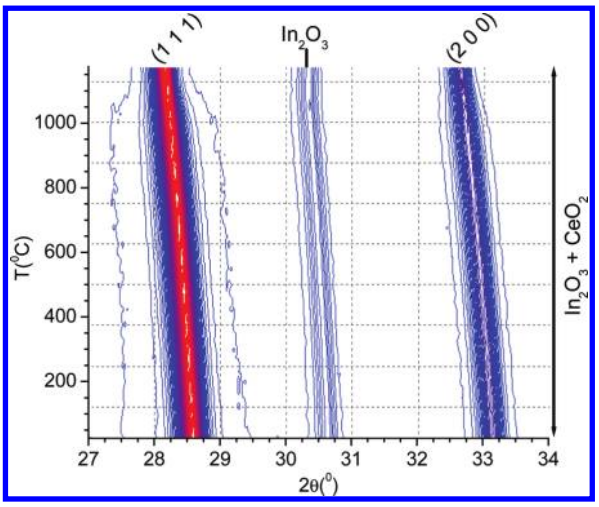

Figure 1. PXRD contour plot illustrating the coexistence of In_2O_3 and CeO_2 between room temperature and 1200 °C in air. The peak shifts of the CeO_2 (111) and (200) reflections and the In_2O_3 (222) reflection at ≈ 30.5° as a function of temperature are due to thermal expansion of the cubic crystal systems with no indication of any reaction. Intensities are shown as constant increments from blue (lowest intensity) to red (highest intensity).

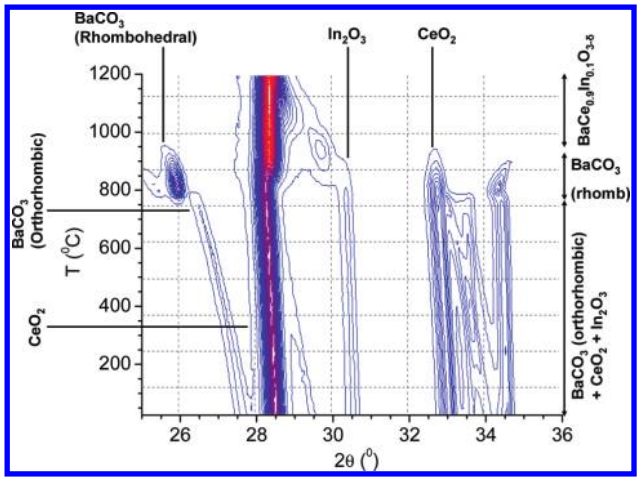

Figure 2. Contour plot of PXRD in the temperature range 25 to 1200 °C at 25 °C increments showing the formation of the perovskite phase $BaCe_{0.9}In_{0.1}O_{3-\delta}$ during the reaction of $BaCO_3$−0.9CeO_2−0.05In_2O_3 in air. Intensities are shown as constant increments from blue (lowest intensity) to red (highest intensity).

sharpen above 1000 °C because of crystalline domain size growth. Most importantly no high temperature intermediates or new phases other than the starting materials are observed during this experiment because of reaction between CeO_2 and In_2O_3; thus, direct In-doping of CeO_2 is not possible.

3.2. Formation of $BaCe_{1-x}In_xO_{3-\delta}$ Perovskites. The preparation of In-doped CeO_2 can be accomplished via the formation of the intermediate In-doped barium cerate perovskites composition of $BaCe_{1-x}In_xO_{3-\delta}$ (x = 0.1, 0.2, 0.3). The formation pathway of $BaCe_{1-x}In_xO_{3-\delta}$ phases during the reaction of stoichiometric amounts of starting materials have been followed via in-situ PXRD from 25 to 1200 °C in 25 °C increments. Figure 2 shows the contour plot of the temperature dependent PXRD during $BaCe_{0.9}In_{0.1}O_{2.95}$ formation in air, and up to approximately 750 °C only the thermal expansion of the starting materials is visible. At 750 °C the transition from

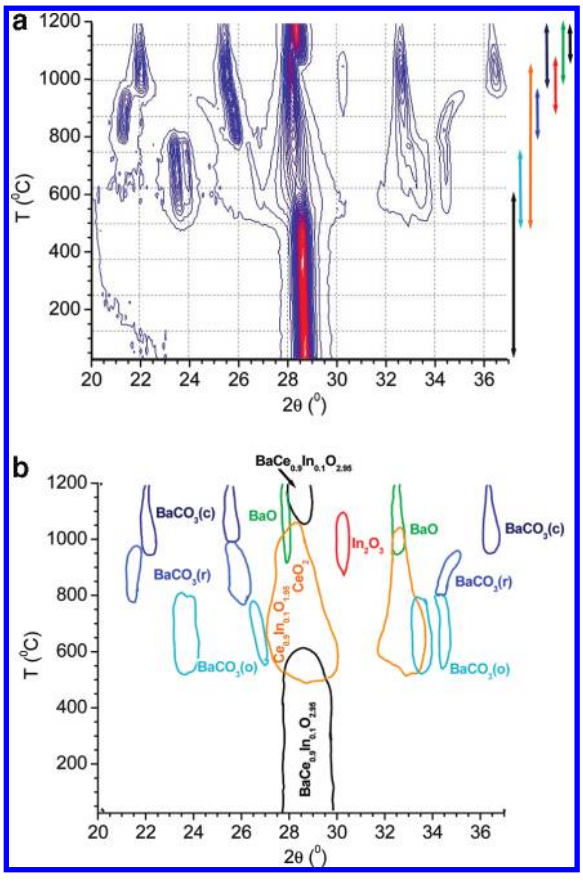

Figure 3. (a) Contour plot of PXRD in the temperature range 25 to 1200 °C at 25 °C increments showing the evolution of phases $Ce_{0.9}In_{0.1}O_{2-\delta}$ under CO_2. The double headed arrows on the right indicate individual phases. The colors are in accordance with (b) phase identification of PXRD contour plot during CO_2 capture reaction of $BaCe_{0.9}In_{0.1}O_{2.95}$. The individual area represents the outlines of the contour plot in panel a. Each phase is represented by an individual color and clearly identified with labels in the same color. The letters in parentheses for $BaCO_3$ stand for (o) = orthorhombic, (r) = rhombohedral, and (c) = cubic.

orthorhombic to rhombohedral $BaCO_3$ is observed, and just below 900 °C, the onset of the $BaCe_{0.9}In_{0.1}O_{2.95}$ formation is observed. At 975 °C the simultaneous disappearance of the In_2O_3 (222) diffraction peak at $2\theta \approx 30.5°$ and the CeO_2 (200) diffraction peak at $2\theta \approx 33°$ can be seen. The absence of the In_2O_3 peak at $T \geq 900$ °C clearly indicates the incorporation of In^{3+} into the final perovskite phase. The high temperature product is a cubic perovskite with < 1% starting material impurities. These impurities can be reacted off during prolonged heating as shown during the bulk synthesis of these materials.

3.3. $BaCe_{1-x}In_xO_{3-\delta}$ Perovskites Decomposition into In-doped CeO_2. In-doped barium cerate perovskite precursors were decomposed in CO_2 flow at high temperatures during an in-situ PXRD experiment. Figure 3a shows the PXRD contour plot of the CO_2 capture reaction carried out on $BaCe_{0.9}In_{0.1}O_{2.95}$. Figure 3b identifies the diffraction peaks of all occurring phases in Figure 3a. The formation of orthorhombic $BaCO_3$ at 475 °C indicates the decomposition of the perovskite phase and results in the $Ce_{0.9}In_{0.1}O_{2-\delta}$ fluorite phase, which is stable up to 825 °C. The $Ce_{0.9}In_{0.1}O_{2-\delta}$ phase undergoes decomposition into CeO_2 and In_2O_3 at 825 °C, which is evident from the appearance of the In_2O_3 peak at ≈30.5° in the contour plot. At 800 °C the orthorhombic to rhombohedral

Scheme 1

$$\begin{aligned}&BaCe_{0.9}In_{0.1}O_{2.95} + CO_2 \xrightarrow{475^0C} Ce_{0.9}In_{0.1}O_{1.95} + BaCO_3(\text{ortho}) \xrightarrow{800^0C} \\ &\xrightarrow{800^0C} Ce_{0.9}In_{0.1}O_{1.95} + BaCO_3(\text{rhom}) \xrightarrow{825^0C} 0.9CeO_2 + 0.05\,In_2O_3 + BaCO_3(\text{romb}) \xrightarrow{900^0C} \\ &\xrightarrow{900^0C} 0.9CeO_2 + 0.05\,In_2O_3 + BaCO_3(\text{cubic}) + BaO \xrightarrow{1100^0C} \\ &\xrightarrow{1100^0C} BaCe_{0.9}In_{0.1}O_{2.95} + CO_2 \quad + \text{minor amounts of unreacted } CeO_2 + In_2O_3 + BaCO_3(\text{cubic})\end{aligned} \tag{1}$$

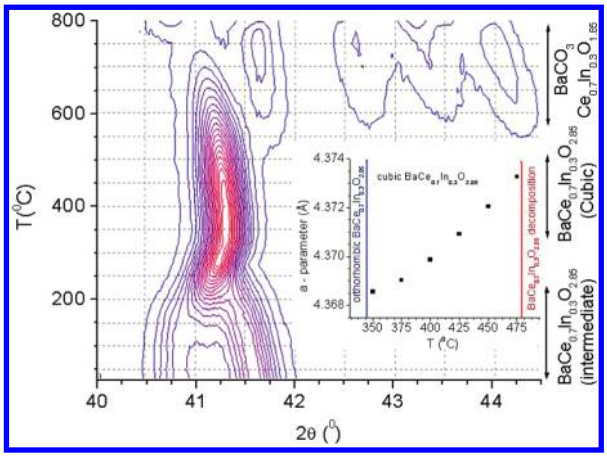

Figure 4. Selected area of the high temperature in-situ PXRD contour plot of $BaCe_{0.7}In_{0.3}O_{2.85}$ reaction in CO_2. Below 350 °C complex peaks splitting is observed. Between 350 and 500 °C a single phase cubic $BaCe_{0.7}In_{0.3}O_{2.85}$ is present. The unit cell expansion of the cubic perovskite is shown in the inset.

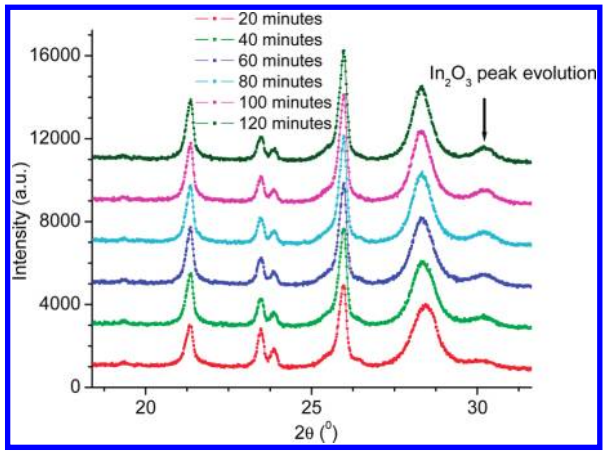

Figure 5. PXRD patterns obtained during isothermal heating of $BaCe_{0.7}In_{0.3}O_{2.85}$ at 800 °C in CO_2.

phase transition of $BaCO_3$ is observed, whereas at 950 °C, $BaCO_3$ becomes cubic, and it seems that equilibrium between $BaCO_3$ and small amounts of BaO exists in this temperature range. The disappearance of In_2O_3 at 1100 °C coincides with the "re"-formation of the In-doped perovskite phase $BaCe_{0.9}In_{0.1}O_{2.95}$ and illustrates the complex reaction sequence. The perovskite phase forms at high temperature again, and this can be explained by the proposed mass unbalanced reaction shown in Scheme 1.The in-situ PXRD supports that at high temperatures, $BaCO_3$ decomposed into BaO and it reacts with readily available CeO_2 and In_2O_3 to the perovskite phase $BaCe_{0.9}In_{0.1}O_{2.95}$ which is now the thermodynamically stable product.

At room temperature the $BaCe_{1-x}In_xO_{3-\delta}$ for $x > 0.1$ structures are orthorhombic or monoclinic, and the indium rich members show a phase transition to cubic symmetry upon heating. The phase pure cubic perovskite undergo the CO_2 capture reactions in CO_2 flow and form the In-doped cerates. The in-situ diffraction contour plot in Figure 4 illustrates the phase transition from orthorhombic to cubic between 300 and 350 °C for $BaCe_{0.7}In_{0.3}O_{3-\delta}$. The thermal expansion of the cubic phase (space group: $Pm\bar{3}m$) between 350 and 500 °C as obtained from single phase Rietveld refinements is illustrated in the inset of Figure 4. Beyond 500 °C $BaCe_{0.7}In_{0.3}O_{3-\delta}$ converts into $Ce_{0.7}In_{0.3}O_{2-\delta}$ and $BaCO_3$. The detailed room temperature structure evolution of the $BaCe_{1-x}In_xO_{3-\delta}$ perovskite phases as a function of In-doping and the structural phase transitions during heating are under investigation and will be reported separately.

The short reaction times during the in-situ experiments result in slightly higher decomposition temperatures of the In-doped CeO_2 samples than the 6 h bulk synthesis

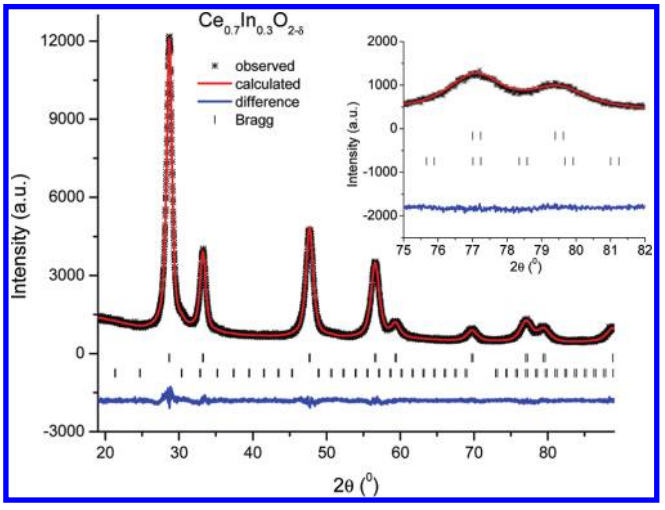

Figure 6. Rietveld plot of $Ce_{0.7}In_{0.3}O_{2-\delta}$ at room temperature. The experimental PXRD are indicated as black crosses, the best fit as a solid red line, the difference as a solid blue line, and the upper set tick marks indicate the Bragg positions of $Ce_{0.7}In_{0.3}O_{2-\delta}$ and the lower set indicates In_2O_3 peak positions.

would provide. This effect is illustrated during the isothermal decomposition of $Ce_{0.7}In_{0.3}O_{2-\delta}$ in CO_2 flow at 800 °C followed in 20 min increments in Figure 5. The onset and growth of the In_2O_3 phase is readily visible as indicated with the (222) diffraction peak. Hence, for the bulk synthesis of $Ce_{0.7}In_{0.3}O_{1.85}$ via the CO_2 capture reaction the temperature had to be lowered to 700 °C to avoid the formation of In_2O_3, whereas $Ce_{0.9}In_{0.1}O_{1.95}$ and $Ce_{0.8}In_{0.2}O_{1.9}$ are stable even at 800 °C.[21]

3.4. Evolution and Stability of $Ce_{1-x}In_xO_{2-\delta}$ (x = 0.1−0.3). Rietveld refinements were carried out against PXRD data of $Ce_{1-x}In_xO_{2-\delta}$ (x = 0.1−0.4) using FullProf.2k.[28] The Rietveld plot of $Ce_{0.7}In_{0.3}O_{1.85}$ is shown in

Table 1. Room Temperature Rietveld Refinement Results for $Ce_{1-x}In_xO_{2-\delta}$ in Space Group $Fm\bar{3}m$ (No. 225)[a]

	x					
	0	0.1	0.2	0.3	0.35	0.4
a (Å)	5.4173(2)	5.4116 (3)	5.4030(4)	5.3932(6)	5.3917(6)	5.3942 (8)
cell volume (Å^3)	158.982(8)	158.48(2)	157.73(2)	156.87(3)	156.74(3)	156.95(3)
d(Ce/In)-O (Å)[b]	2.34574(8)	2.3433(1)	2.3396(2)	2.3353(3)	2.3347(3)	2.3357(4)
In_2O_3 (mass %)	0	<1.0	<1.0	1.0	7	16
R_p	3.62	3.50	2.90	3.05	3.05	3.20
R_{wp}	4.71	4.46	3.69	3.86	3.83	4.08
χ^2	2.76	2.32	1.88	1.72	1.93	2.19
no. of parameters	25	25	25	25	26	26
no. of data points	4247	4247	4247	4247	4247	4247

[a] Ce^{4+}/In^{3+} are disordered on 4*a* (0,0,0) site and O^{2-} located on 8*c* (1/4, 1/4, 1/4) site. Note that $x < 0.3$ are single phase refinements with 25 parameters, whereas $x \geq 0.3$ is two phase refinements with 26 parameters. The refined parameters include background, cubic cell parameter *a*, asymmetry parameters, and peak shape parameters for the pseudo-Voigt profile. [b] The Shannon radii[24] at 8-fold oxygen coordination number (CN) of Ce(CN = 8)$^{4+}$, In(CN= 8)$^{3+}$, and O(CN = 4)$^{2-}$ predict the bond distances d(Ce−O) = 2.35 Å and d(In−O) = 2.30 Å, and these agree very well with our experimental results for $Ce_{1-x}In_xO_{2-\delta}$.

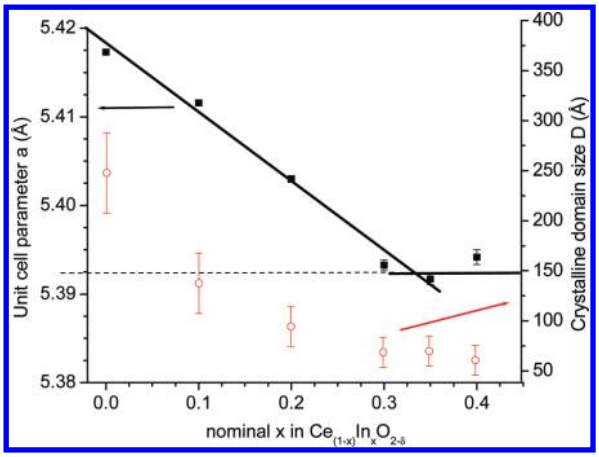

Figure 7. Solid black squares: cubic unit cell parameter evolution in $Ce_{1-x}In_xO_{2-\delta}$. The solid black lines are only a guide to the eye. The samples with nominal compositions $x = 0.35$ and 0.40 contain In_2O_3 as a second phase. Open red circles: isotropic crystalline domain size evolution in $Ce_{1-x}In_xO_{2-\delta}$ as obtained with the Scherrer eq 3.

Figure 6, and the refinement results are provided in Table 1. In-doped CeO_2 crystallize in the fluorite structure in space group $Fm\bar{3}m$(No. 225) with Ce^{4+}/In^{3+} disorder on the 4*a* (0,0,0) site and oxide anions located on the 8*c* (1/4, 1/4, 1/4) site with disordered oxide defects. During the Rietveld refinements the background was described with linear interpolations between 17 refined background points, the unit cell constants, pseudo-Voigt peak shape parameters, peak asymmetries, and scale factors have been refined. Figure 7 represents the variation of the cubic unit cell parameter for $Ce_{1-x}In_xO_{2-\delta}$ as a function of nominal indium content. As expected with increasing indium content, the unit cell of the fluorite phase contracts owing to the smaller ionic radius of In^{3+} compared to Ce^{4+} and the smaller concentration of oxide anions.[24] It was identified that up to $x = 0.3$, $Ce_{1-x}In_xO_{2-\delta}$ can be synthesized as a single phase without the presence of In_2O_3 impurity. All samples with $x > 0.3$ resulted in two phase products consisting of $Ce_{0.7}In_{0.3}O_{1.85}$ and excess In_2O_3 as illustrated for $x = 0.35$ and 0.4. The unit cell dimensions do not change significantly beyond $x = 0.3$, thus indicating that $x = 0.3$ is the maximum In content in $Ce_{1-x}In_xO_{2-\delta}$ prepared by the CO_2 capture route.

Notably the diffraction peaks of the In-doped phases show broadening with increasing indium content because of decreasing crystalline domain sizes. No significant strain induced broadening has been observed. The isotropic crystalline domain sizes were estimated using the Scherrer eq 3, that is,

$$D = 0.9\lambda/(B\cos\theta) \quad (3)$$

where D is the domain size, B the integral breadth, λ the wavelength, and θ the diffraction angle. The original CeO_2 starting material has crystalline domain sizes in excess of 600 Å whereas the same CeO_2 after the CO_2 capture reaction shows nanosized crystalline domains of 250(40) Å. Upon indium doping the domain sizes decrease monotonically from $x = 0$ to $x = 0.3$ and plateau beyond $x = 0.3$ as shown in Figure 7. Note that the crystalline domain size and the cubic unit cell parameter plateau simultaneously at $x \geq 0.3$ with $D = 70$ (15) Å. This clearly indicates that the domain sizes are controlled by the indium content in the CeO_2 phase and are only limited by the stability range of fluorite-type phase.

3.5. Competition between CO_2 Capture Reaction and $Ce_{1-x}In_xO_{2-\delta}$ Decomposition. The formation of pure bulk samples of $Ce_{1-x}In_xO_{2-\delta}$ ($x = 0.1$ - 0.3) requires temperatures from 600 to 700 °C during the CO_2 capture reaction. The $Ce_{1-x}In_xO_{2-\delta}$ bulk samples undergo decomposition into their binary oxides at approximately 800 °C for $x < 0.3$ and at ≤700 °C for $x \geq 0.3$. The in-situ PXRD data during the CO_2 capture reaction provide intriguing insights into the formation temperatures (T_{form}) of $Ce_{1-x}In_xO_{2-\delta}$. The T_{form} for $x = 0.1$, 0.2 is 475 °C, and for $x = 0.3$ it is 500 °C, whereas the decomposition temperatures (T_{decomp}) of $Ce_{1-x}In_xO_{2-\delta}$ for $x = 0.1$ is 825 °C and for $x = 0.2$ and 0.3 are 800 and 775 °C, respectively, as determined by the first appearance of In_2O_3 (Figures 3a, b). To obtain pure $Ce_{1-x}In_xO_{2-\delta}$ bulk samples, the reactions need to be carried out approximately 100 °C above T_{form}. The formation and decomposition temperatures converge toward each other for increased indium doping levels, and consequently a maximum value for In-doping is observed during the preparation of $Ce_{1-x}In_xO_{2-\delta}$ by means of CO_2 capture. On the basis of this finding, we suggest that larger indium concentrations in CeO_2 are only achievable if an intermediate is used that can form the $Ce_{1-x}In_xO_{2-\delta}$ phases at lower temperatures. All reported $Ce_{1-x}In_xO_{2-\delta}$ phases are metastable, and thus can only be accessed through low temperature CO_2 mediated preparation routes.

4. Conclusions

The phase evolution of $BaCe_{1-x}In_xO_{3-\delta}$ and the CO_2 capture reaction leading to the formation of $Ce_{1-x}In_xO_{2-\delta}$ has been investigated via the in-situ PXRD method. The complex reaction pathway during the 2 step synthesis has been discussed in detail. This has allowed a better understanding of the formation pathway as well as of the metastability of these phases. The $Ce_{1-x}In_xO_{2-\delta}$ has been successfully synthesized up to $x = 0.3$ without In_2O_3 impurities. Lattice constants obtained via the Rietveld refinements of $Ce_{1-x}In_xO_{2-\delta}$ followed the Shannon radii trend and illustrate the maximum indium concentration in $Ce_{1-x}In_xO_{2-\delta}$. The crystalline domain sizes decrease with increasing indium-doping and reach a minimum $D = 70(15)$ Å for $x \geq 0.3$. The CO_2 capture reaction opens up an elegant synthetic method for the preparation of doped fluorite-type phase via the ($B^{/}B^{//}$) cation disordered $Ba(B^{/}_{1-x}B^{//}_{x})O_3$ perovskites. The decomposition into $BaCO_3$ and $B^{/}_{1-x}B^{//}_{x}O_{2-\delta}$ is thermodynamically driven by the formation of $BaCO_3$ in carbon dioxide and provides access to the metastable $B^{/}_{1-x}B^{//}_{x}O_{2-\delta}$ phases.

Acknowledgment. V.T. and M.B. thank the Natural Sciences and Engineering Research Council of Canada (NSERC) for operating and infrastructure support. We also thank the Canada Foundation for Innovation (CFI) for providing funding for the X-ray facility. S.P.S. is thankful to the University of Manitoba for a graduate fellowship (UMGF).